

Perturbational and nonperturbational inversion of Love-wave velocities

Matthew M. Haney¹ and Victor C. Tsai²

ABSTRACT

We describe a set of MATLAB codes to forward model and invert Love-wave phase or group velocities. The forward modeling is based on a finite-element method in the frequency-wavenumber domain, and we obtain the different modes with an eigenvector-eigenvalue solver. We examine the issue of parasitic modes that arises for modeling Love waves, in contrast to the Rayleigh wave case, and how to discern parasitic from physical modes. Once the matrix eigenvector-eigenvalue problem has been solved for Love waves, we show a straightforward technique to obtain sensitivity kernels for S-wave velocity and density. In practice, the sensitivity of Love waves to density is relatively small and inversions only aim to estimate the S-wave velocity. Two types of inversion accompany the forward-modeling codes: One is a perturbational scheme for updating an initial model, and the other is a nonperturbational method that is well-suited for defining a good initial model. The codes are able to implement an optimal nonuniform layering designed for Love waves, invert combinations of phase and group velocity measurements of any mode, and seamlessly handle the transition from guided to leaky modes below the cutoff frequency. Two software examples demonstrate use of the codes at near-surface and crustal scales.

INTRODUCTION

Surface waves interrogate the earth over different depths at each frequency, and this property has led to their popularity for imaging near-surface structure. In active source seismology, Rayleigh waves are more commonly used due to their excitation by vertical sources and ability to be recorded by 1C vertical receivers. Love waves require horizontal sources and sensors; however, their dispersion curves

are unaffected by the P-wave velocity in the subsurface and are therefore advantageous for imaging purely S-wave structure (Xia et al., 2012). Similarly, ocean-bottom recordings of Love waves are unaffected by the presence of the water layer (Muyzert, 2007). Another advantage of Love waves is that their dispersion curves are often simpler than Rayleigh-wave dispersion curves (Jay et al., 2012; Xia et al., 2012). The issue of horizontal sources for analyzing Love waves can be overcome in passive methods by using ambient seismic noise, which can take the form of traffic noise (Behm et al., 2014; Nakata, 2016) or volcanic tremor (Chouet et al., 1998; Lanza et al., 2016).

Several methods have been put forward for modeling the phase velocities and mode shapes of Love waves (Takeuchi and Saito, 1972; Aki and Richards, 1980; Saito, 1988; Herrmann and Ammon, 2004; Denolle et al., 2012; Herrmann, 2013; Hawkins, 2018). Here we describe an approach for modeling and inversion of Love wave dispersion based on finite elements, which is known in surface-wave applications as the thin-layer method (Kausel, 2005). Haney and Tsai (2017) provide details of the thin-layer method for modeling of Rayleigh waves and show how perturbational inversion naturally follows from the finite-element formulation. We do the same here for Love waves, taking care to emphasize differences that arise for Love waves compared to Rayleigh waves. We closely follow the presentation in Haney and Tsai (2017) for Rayleigh waves and provide a MATLAB software package with two examples of Love wave inversion.

In addition to perturbational inversion, we also describe a new type of nonperturbational inversion of Love waves based on the recently derived Dix-type relations for surface waves (Haney and Tsai, 2015). Nonperturbational inversion based on the Dix-type relation is well-suited for defining a good initial model for further refinement by perturbational methods. The hallmark of the Dix equation in reflection seismology (Dix, 1955) is the proportionality of squared stacking velocities and squared interval velocities. Haney and Tsai (2015) show that this approximation carries over to squared phase velocities and squared S-wave velocities for surface waves. The extension to squared group velocities has been

Peer-reviewed code related to this article can be found at <http://software.seg.org/2020/0002>.

Manuscript received by the Editor 30 January 2019; revised manuscript received 9 August 2019; published ahead of production 16 October 2019; published online 22 November 2019.

¹Alaska Volcano Observatory, U.S. Geological Survey Volcano Science Center, Anchorage, Alaska 99508, USA. E-mail: mhaney@usgs.gov.

²Brown University, Department of Earth, Environmental and Planetary Sciences, Providence, Rhode Island 02912, USA. E-mail: victor_tsai@brown.edu.

© 2020 Society of Exploration Geophysicists. All rights reserved.

subsequently presented by Haney and Tsai (2017). The Dix-type relations for surface waves are derived under the assumption of either a background homogeneous medium or power-law velocity profile. Tsai and Atiganyanun (2014) demonstrate that power-law velocity profiles are particularly applicable for the shallow subsurface and that surface waves in such media have self-similar characteristics. In fact, for Love waves, the Dix-type relation is only possible for a background power-law velocity profile because Love waves do not exist in a homogeneous half-space.

FORWARD MODELING OF LOVE DISPERSION

The use of the finite-element method for modeling Love waves follows many of the same considerations discussed previously in Haney and Tsai (2017) for Rayleigh waves. Kausel (2005) shows details for the case of SH-waves in a layered medium, and the general approach has been called the thin-layer method because the depth discretization must be dense enough to adequately sample the surface wave eigenfunction in depth. These types of considerations apply to all discrete ordinate methods, including finite differences and spectral elements (Hawkins, 2018). Here, we review the main aspects of finite elements for modeling Love waves.

The finite-element model is specified by N thin layers, or elements, with $N + 1$ nodes between the elements. The most shallow node is at the stress-free surface of the earth model, and the displacement of the deepest node is set to zero. The horizontal eigenfunction in the transverse direction (l_1 in the notation of Aki and Richards, 1980) must decay considerably with depth before encountering the base of the model in order for this approximation to be accurate. When the model is deep enough, the true eigenfunction would be close to zero at the deepest node; therefore, fixing the eigenvector at zero (i.e., the Dirichlet boundary condition) causes negligible error. To test if the model is deep enough, we require that the depth of the model be greater than the wavelength ℓ of the Love waves multiplied by the mode number

$$L > m\ell, \quad (1)$$

where $m = 1$ is the fundamental mode, $m = 2$ is the first overtone, and so on.

Haney and Tsai (2017) explain the inequality in equation 1 in terms of the sensitivity depth of surface waves, which is the depth at which most surface wave sensitivity to the S-wave velocity exists. Xia et al. (1999) numerically test fundamental-mode Rayleigh waves for a particular depth model and find the sensitivity depth to be approximately equal to 0.63ℓ . From this depth, Xia et al. (1999) obtain a crude estimate of the S-wave velocity structure by taking the fundamental-mode Rayleigh-wave phase velocity for a wavelength of ℓ , multiplying it by a factor of 0.88, and mapping it to a depth of 0.63ℓ . Xia et al. (1999) find the empirical factors of 0.63 and 0.88 through forward modeling. We return to this simple, data-driven method of building a depth model in a later section. By using a Dix-type relation for surface waves, Haney and Tsai (2015) demonstrate that the fundamental-mode Rayleigh sensitivity depth in a power-law S-wave velocity profile (i.e., one in which the S-wave velocity $\beta(z) \propto z^n$ and $n < 1$) is well-approximated by 0.5ℓ , close to the estimate of 0.63ℓ by Xia et al. (1999). Haney and Tsai (2015) further find that the fundamental-mode Love wave has an even shallower sensitivity depth of 0.25ℓ in power-law S-wave profiles. From these sensitivity depth considerations, the inequality in equation 1 can be interpreted for the fundamental

Love-wave mode ($m = 1$) to mean that the depth extent of the model must be four times the sensitivity depth. Including the general factor of m in equation 1 covers the case of higher modes, as discussed by Haney and Tsai (2017).

Before testing to ensure the inequality in equation 1 is satisfied, we first need to solve the Love-wave eigenproblem. We organize the N unknown nodal displacements of the transverse horizontal eigenfunction (l_1) in a vector:

$$\mathbf{v} = [\dots l_1^{K-1} \ l_1^K \ l_1^{K+1} \ \dots]^T. \quad (2)$$

As shown by Kausel (2005), the Love wave eigenvector is then given by a generalized linear eigenvalue problem in terms of the squared wavenumber k^2 and squared frequency ω^2

$$(k^2\mathbf{B}_2 + \mathbf{B}_0)\mathbf{v} = \omega^2\mathbf{M}\mathbf{v}, \quad (3)$$

where the stiffness matrices \mathbf{B}_2 and \mathbf{B}_0 are only dependent on shear modulus μ and the mass matrix \mathbf{M} only depends on density ρ . The exact structure of matrices \mathbf{B}_2 , \mathbf{B}_0 , and \mathbf{M} is discussed in detail by Kausel (2005) for the case of SH-waves. Note that equation 3 has a similar form as the Rayleigh-wave case shown in Haney and Tsai (2017), except that there is no first-order term in the wavenumber. The presence of the first-order term in the Rayleigh-wave case causes the eigenproblem to be quadratic, instead of linear. Once equation 3 has been solved for eigenvalue k^2 and eigenvector \mathbf{v} (with specified ω^2), the square root of the eigenvalue gives the wavenumber of the mode. The group velocity U of any mode can be found from its eigenvalue and eigenvector from the relation (Haney and Douma, 2011):

$$U = \frac{\delta\omega}{\delta k} = \frac{\mathbf{v}^T\mathbf{B}_2\mathbf{v}}{c\mathbf{v}^T\mathbf{M}\mathbf{v}}, \quad (4)$$

where c is the phase velocity. Equation 4 can be derived from the Rayleigh-wave group-velocity expression (Haney and Tsai, 2017) by setting the first-order term, which appears for Rayleigh waves, to zero.

Oftentimes, we are only interested in the fundamental mode or a few of the lowest order modes when solving equation 3. In that case, solving for all of the modes would be inefficient. We take an approach for finding the eigenvalue and eigenvector of a given mode as discussed by Haney and Tsai (2017) for Rayleigh waves. We use the MATLAB function *eigs*, a solver based on the ARPACK linear solver (Lehoucq et al., 1998), which can find an eigenvalue (or group of eigenvalues) closest to a particular value. The fundamental mode has the largest k eigenvalue; therefore, we can specify that mode if we have an upper bound on the fundamental-mode eigenvalue. Finding an upper bound on the fundamental-mode eigenvalue is more straightforward for Love waves than the method described by Haney and Tsai (2017) for Rayleigh waves. The upper bound is found from the minimum value of S-wave velocity in the model β_{\min} , which gives an upper bound of ω/β_{\min} for the wavenumber. By asking the eigensolver to return the mode closest to this upper bound, we would obtain the fundamental Love-wave mode. If we ask for the two closest modes, then we would obtain the fundamental mode and the first overtone. Although it is not possible to obtain a higher order mode without also asking for all the lower order modes below it, this approach is more efficient than computing all the modes.

A complication encountered for Love waves compared to the Rayleigh-wave case is that there can be parasitic or artificial numerical modes with eigenvalues interspersed among the physical Love wave modes. These parasitic or artificial modes are typical of those encountered in finite-element or finite-difference codes, which sometimes give rise to instabilities in the time domain (Haltiner and Williams, 1980; Marfurt, 1984; Haney, 2007). They have mode shapes with parts that are close to the spatial Nyquist wavenumber in depth, and we can detect them based on that property. To handle the possibility of parasitic modes, we test the output after solving equation 3 to see if any parasitic modes were returned. If parasitic modes were returned, we solve equation 3 again and keep solving it until we obtain all of the lowest order modes of interest. We note that similar parasitic modes have not been encountered for the Rayleigh wave case; however, to be careful, a similar scheme for detecting parasitic modes could be applied for Rayleigh waves.

A primary consideration for accurate modeling concerns the thickness of the finite elements. The simplest approach would be to use uniformly thick elements; however, such elements would oversample the eigenfunctions below their sensitivity depths. At those depths, the eigenfunctions are slowly varying, decaying exponentials. As a rule of thumb, we have found that sampling the eigenfunctions at least five times per wavelength for all depths above the sensitivity depth is adequate. This leads to the following requirement:

$$\ell > 5h_s, \quad (5)$$

where h_s is the element thickness at all depths shallower than the maximum sensitivity depth, which for Love waves in a power-law velocity profile is approximately given by $z = 0.25m\ell$. Based on these considerations, Haney and Tsai (2017) show how to obtain an optimal layering for Rayleigh waves — one that provides adequate sampling shallower than the sensitivity depth but that does not unnecessarily oversample the model deeper than it. This same type of nonuniform grid can be used for Love waves as well. Such a depth discretization has in fact also been used by Ma and Clayton (2016) for Rayleigh- and Love-wave inversion.

A final issue is whether guided Love-wave modes even exist for a particular model at a certain frequency. For example, Love waves do not exist for a homogeneous half-space; therefore, the codes should indicate this if they are given a homogeneous model. Our approach to this problem is the same as applied to Rayleigh waves in Haney and Tsai (2017): The eigenfunction found by the solver is tested, and if it does not meet a criterion to be considered a guided wave, NaNs are returned for the eigenvalue and eigenvector. Subsequent functions and scripts can detect the NaNs and avoid using those frequency-velocity pairs because the model does not support guided waves at those frequencies. The criterion to be considered a guided wave is that the depth integral of the absolute value of the eigenfunction over the upper half of the depth model must be at least three times larger than the depth integral of the same function over the lower half of the model. The factor of three comes from a linearly decreasing function with depth, which is fixed at zero at the base of the model. In that case, the ratio of the depth integrals would be exactly three. Thus, the criterion tests whether the eigenfunction decays faster than linearly as a function of depth and classifies it as a guided mode if it does. This test has proven successful in practice for discriminating guided from nonguided modes.

PERTURBATIONAL INVERSION OF DISPERSION CURVES

The Love-wave eigenvalue-eigenvector problem, shown in equation 3, has the same form as the Rayleigh-wave case, except that one term, which is linear in the wavenumber, is missing. Therefore, many of the results for Love waves can be obtained from the Rayleigh wave formulas presented in Haney and Tsai (2017) as a special case. For example, the perturbation in the Love-wave phase velocity of a particular mode due to perturbations in shear modulus and density at a fixed frequency is given by

$$\frac{\delta c}{c} = \frac{1}{2k^2 U c \mathbf{v}^T \mathbf{M} \mathbf{v}} \times \left(\sum_{i=1}^N \mathbf{v}^T \frac{\partial(k^2 \mathbf{B}_2 + \mathbf{B}_0)}{\partial \mu_i} \mathbf{v} \delta \mu_i - \omega^2 \sum_{i=1}^N \mathbf{v}^T \frac{\partial \mathbf{M}}{\partial \rho_i} \mathbf{v} \delta \rho_i \right). \quad (6)$$

When evaluated over many frequencies, this equation results in a linear matrix-vector relation between the perturbed phase velocities and the perturbations in shear modulus and density

$$\frac{\delta \mathbf{c}}{\mathbf{c}} = \mathbf{K}_\mu^c \frac{\delta \boldsymbol{\mu}}{\boldsymbol{\mu}} + \mathbf{K}_\rho^c \frac{\delta \boldsymbol{\rho}}{\boldsymbol{\rho}}, \quad (7)$$

where \mathbf{K}_μ^c and \mathbf{K}_ρ^c are the phase velocity kernels for shear modulus and density, respectively. Note that the kernels shown here are for relative perturbations.

Although equation 7 is a linear relation between phase-velocity perturbations and perturbations in shear modulus and density, in practice, Love waves are typically only inverted for depth-dependent S-wave velocity profiles. This is because Love-wave velocities are mostly dependent on the S-wave velocity in the subsurface. To find the linear relation between phase-velocity perturbations and S-wave velocity, we use the following relation valid to first order:

$$\frac{\delta \boldsymbol{\mu}}{\boldsymbol{\mu}} = 2 \frac{\delta \boldsymbol{\beta}}{\boldsymbol{\beta}} + \frac{\delta \boldsymbol{\rho}}{\boldsymbol{\rho}}. \quad (8)$$

Substituting equation 8 into equation 7 gives

$$\frac{\delta \mathbf{c}}{\mathbf{c}} = 2 \mathbf{K}_\mu^c \frac{\delta \boldsymbol{\beta}}{\boldsymbol{\beta}} + (\mathbf{K}_\mu^c + \mathbf{K}_\rho^c) \frac{\delta \boldsymbol{\rho}}{\boldsymbol{\rho}}. \quad (9)$$

Finally, by assuming no perturbations in the density model, this yields

$$\frac{\delta \mathbf{c}}{\mathbf{c}} = 2 \mathbf{K}_\mu^c \frac{\delta \boldsymbol{\beta}}{\boldsymbol{\beta}} = \mathbf{K}_\beta^c \frac{\delta \boldsymbol{\beta}}{\boldsymbol{\beta}}. \quad (10)$$

Thus, the S-wave velocity kernel is twice the value of the μ kernel. The assumption of no density perturbations means that the density is fixed during inversion to its value specified in the initial model.

When considering group velocities, the sensitivity kernel is related to the phase-velocity kernel (Rodi et al., 1975) as

$$\mathbf{K}_\beta^U = \mathbf{K}_\beta^c + \frac{U \omega}{c} \frac{\partial \mathbf{K}_\beta^c}{\partial \omega}. \quad (11)$$

In the numerical codes described later, the derivative of the phase-velocity kernel with respect to frequency in equation 11 is evaluated

numerically using second-order-accurate differencing. A similar linear relation as shown in equation 10 can thus be set up for the group velocity

$$\frac{\delta \mathbf{U}}{\mathbf{U}} = \mathbf{K}_\beta^U \frac{\delta \boldsymbol{\beta}}{\boldsymbol{\beta}}. \quad (12)$$

In the numerical codes, the linear relations shown in equations 10 and 12 are set up in terms of absolute perturbations instead of relative perturbations. Denoting the group-velocity kernel in this case as \mathbf{G}_β^U , the absolute perturbation kernel can be given in terms of the relative perturbation kernel as

$$\mathbf{G}_\beta^U = \text{diag}(\mathbf{U}) \mathbf{K}_\beta^U \text{diag}(\boldsymbol{\beta})^{-1}, \quad (13)$$

where $\text{diag}(\mathbf{U})$ is a matrix with the vector \mathbf{U} placed on the main diagonal and off-diagonal entries equal to zero. The same form applies to the computation of absolute phase-velocity kernels from the relative kernels.

Regularization is necessary for phase and/or group velocity inversion, and we adopt a simple strategy based on weighted damped least squares. Data covariance and model covariance matrices \mathbf{C}_d and \mathbf{C}_m are chosen as shown in Gerstoft et al. (2006). The data covariance matrix is assumed to be a diagonal matrix

$$\mathbf{C}_d(i, i) = \sigma_d(i)^2, \quad (14)$$

where $\sigma_d(i)$ is the data standard deviation of the i th phase or group velocity measurement. The model covariance matrix has the form

$$\mathbf{C}_m(i, j) = \sigma_m^2 \exp(-|z_i - z_j|/D), \quad (15)$$

where σ_m is the model standard deviation, z_i and z_j are the depths at the top of the i th and j th elements, and D is a smoothing distance or correlation length. In the numerical codes, the model standard deviation is given as a user-supplied factor times the median of the data standard deviations.

Given these covariance matrices, we use the algorithm of total inversion (Tarantola and Valette, 1982; Muzyert, 2007) to invert a general collection of phase and group velocities of any Love-wave mode. Thus, we denote the kernel \mathbf{G}_β because in general it may contain phase- and group-velocity measurements. The n th model update $\boldsymbol{\beta}_n$ is calculated by forming the augmented system of equations (Snieder and Trampert, 1999; Aster et al., 2004):

$$\begin{aligned} & \begin{bmatrix} \mathbf{C}_d^{-1/2} \\ 0 \end{bmatrix} (\mathbf{U}_0 - \mathbf{f}(\boldsymbol{\beta}_{n-1}) + \mathbf{G}_\beta (\boldsymbol{\beta}_{n-1} - \boldsymbol{\beta}_0)) \\ &= \begin{bmatrix} \mathbf{C}_d^{-1/2} \mathbf{G}_\beta \\ \mathbf{C}_m^{-1/2} \end{bmatrix} (\boldsymbol{\beta}_n - \boldsymbol{\beta}_0), \end{aligned} \quad (16)$$

where \mathbf{U}_0 is the phase/group velocity data, \mathbf{f} is the (nonlinear) forward-modeling operator, and n ranges from one to whenever the stopping criterion is met or the maximum allowed number of iterations is reached. The stopping criterion used here is based on the χ^2 value (Gouveia and Scales, 1998)

$$\chi^2 = (\mathbf{f}(\boldsymbol{\beta}_n) - \mathbf{U}_0)^T \mathbf{C}_d^{-1} (\mathbf{f}(\boldsymbol{\beta}_n) - \mathbf{U}_0) / F, \quad (17)$$

where F is the number of measurements (the number of frequencies where the Love phase/group velocities have been measured). The iteration is terminated when the χ^2 value falls within a user-prescribed window. In the code examples shown later, this window is set for χ^2 between 1.0 and 1.5. The inversion given in equation 16 is then passed to a conjugate gradient solver (Paige and Saunders, 1982) and iterated to convergence, or when the maximum allowed number of iterations is reached. We use reduction steps in the iteration if an updated model increases the χ^2 value from the previous mode. Such a reduction step involves scaling down the length of the gradient step between the previous model and the potential update by a factor of one-half. This reduction is repeated until the χ^2 of the update is less than the previous model or the maximum allowed number of reduction steps is reached.

NONPERTURBATIONAL INVERSION OF DISPERSION CURVES

In addition to perturbational inversion, the codes include the capability of building an initial model through nonperturbational inversion based on the Dix-type relation for fundamental-mode surface waves (Haney and Tsai, 2015). Such a relation states that, to a good approximation, squared observable velocities are linearly proportional to squared medium velocities. Thus, the Dix-type relation leads to a linear inverse problem:

$$\mathbf{c}^2 = \mathbf{G} \boldsymbol{\beta}^2, \quad (18)$$

where \mathbf{G} is the kernel relating the squared shear velocities to the squared phase velocities. A Dix-type relation also exists for group velocities (Haney and Tsai, 2017). Several different Dix-type relations have been derived for fundamental-mode Rayleigh waves under the assumption of either a homogeneous half-space or a power-law shear-velocity profile. For Love waves, this is only possible for power-law shear-velocity profiles because Love waves do not exist in a homogeneous half-space.

Details of the inversion methodology are similar to the Rayleigh wave case discussed by Haney and Tsai (2017). Because equation 18 represents a linear inverse problem, it is solved in a single iteration (Tarantola and Valette, 1982). Knowledge of the model correlation length and model standard deviation may be difficult to know a priori, and the Dix-type relation is an approximation. As a result, in the implementation of nonperturbational inversion, we scan over many values of each regularization parameter and then average the models that fit the data to within the acceptable χ^2 window. If no acceptable models are found over the range of the regularization parameters, the user is prompted to expand it. We use the same forms for the data and model covariance matrices as for the perturbational inversion described in the previous section. This yields an augmented version of equation 18 given by

$$\begin{bmatrix} \mathbf{C}_d^{-1/2} \mathbf{G} \\ \mathbf{C}_m^{-1/2} \end{bmatrix} \boldsymbol{\beta}^2 = \begin{bmatrix} \mathbf{C}_d^{-1/2} \mathbf{c}^2 \\ \mathbf{C}_m^{-1/2} \boldsymbol{\beta}_0^2 \end{bmatrix}, \quad (19)$$

where $\boldsymbol{\beta}_0^2$ is the S-wave velocity model obtained using the data-driven model-building method described by Xia et al. (1999). As discussed earlier, Xia et al. (1999) obtain an estimate of the S-wave velocity profile by mapping the phase velocity of the fundamental-mode Rayleigh wave with a wavelength of ℓ to a S-wave velocity at

the sensitivity depth. For Love waves, under the assumption of a power-law shear-velocity profile, this process is modified by taking the fundamental-mode Love-wave phase velocity for a wavelength of ℓ and mapping it to the sensitivity depth, which for Love waves is approximately 0.25ℓ (Haney and Tsai, 2015). We have implemented a version of this data-driven method using robust extrapolation to expand the model above and below the minimum and maximum sensitivity depths, respectively. The Dix-type inversion shown in equation 19 improves upon the simple data-driven model. A current limitation of the Dix method is that it has only been formulated for fundamental-mode data.

SOFTWARE EXAMPLES

The entire package of codes, called the LOVEE package (LOVE waves with Eigenvector-Eigenvalue solver), consists of seven MATLAB functions, eight MATLAB scripts, and one text README file. Two phase-velocity inversion examples are included with the package. The first inversion example uses noisy synthetic fundamental-mode data from the near-surface MODX model (Xia et al., 1999), an initial model defined by Dix inversion of Love waves under the power-law velocity profile assumption, and an optimal nonuniform layering to find an acceptable velocity model. The second example performs inversion with a crustal-scale model using phase velocities measured for fundamental and first higher mode Love waves between 0.1 and 0.9 Hz. The crustal model is the same one used for Rayleigh wave examples in Haney and Tsai (2017). Although the example uses the same model, the initial model is not a homogeneous half-space as used in Haney and Tsai (2017) because Love waves do not exist for such a model. Instead, the initial model is computed from Dix inversion of fundamental-mode Rayleigh-wave data under the assumption of a homogeneous half-space. Rayleigh waves are better at building an initial model than Love waves for this example because the heterogeneity is relatively weak, and thus the Love-wave Dix relation assuming a power-law velocity profile is not suitable. This crustal-scale model has the

added complexity of radial anisotropy in one of the layers, with the SV-wave velocity (the one affecting Rayleigh waves) set 18% lower than the SH-wave velocity (the one affecting Love waves). Such radial anisotropy has been shown to be relevant in the subsurface at volcanoes (Jaxybulatov et al., 2014). Executing the codes associated with these inversion examples reproduces Figures 1, 2, 3, 4, 5, and 6. Each code has been successfully run using MATLAB version R2017b on a laptop computer with 16 GB RAM and a 2.3 GHz clock speed in less than 70 s. The signal processing toolbox add-on to the basic MATLAB program is needed to run the codes. The source codes themselves contain extensive comments for clarity.

The first inversion example uses the near-surface MODX model (Xia et al., 1999), which Haney and Tsai (2017) also analyzed for the Rayleigh wave case. In contrast to Rayleigh waves, no assumption regarding the value of Poisson's ratio is needed for Love wave inversion. To run the example, we execute the following four MATLAB scripts:

```
>> make_synthetic_ex1
>> make_initial_model_dix_ex1
>> lovee_invert
>> plot_results_ex1
```

The first script computes synthetic Love-wave phase velocities over the band from 3 to 30 Hz for the fundamental mode with 2% noise added. The next command finds an initial model using the Dix method for Love waves with the power-law velocity-profile formulation (Haney and Tsai, 2015). The synthetic data are then inverted with the perturbational code in the third step, and an acceptable model fitting the data to within the noise level is found after only one iteration because the initial model is close to the true one. Figures 1–3 are generated by the last script and show details of the inversion. Figure 1 plots the initial, final, and true models, and although the initial model is close to the true model, the perturbational inversion

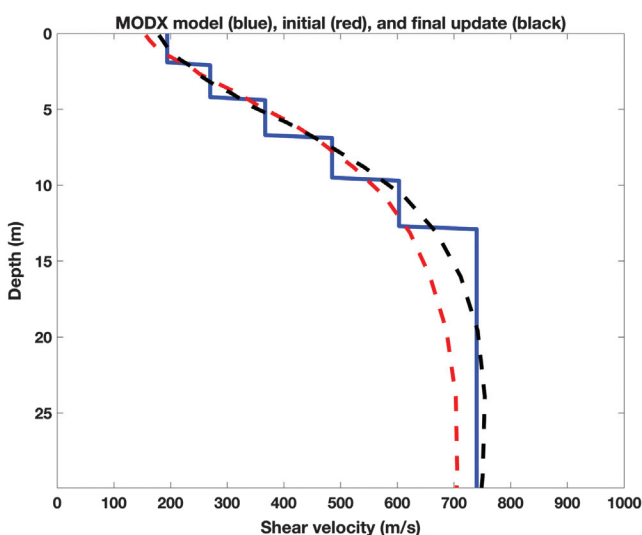


Figure 1. Shear velocity depth models for the MODX example using phase velocities: true model (solid blue), initial model (dashed red), and inverted model (dashed black). The initial model is generated using a Dix-type phase inversion for Love waves.

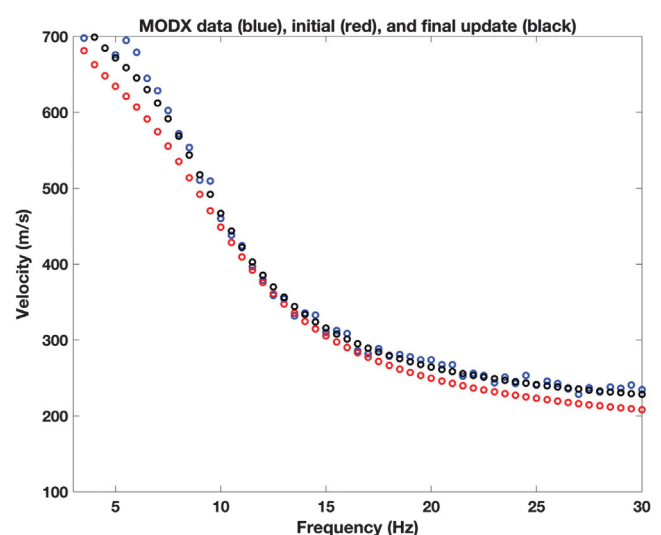


Figure 2. Phase velocity dispersion curves for the MODX example: noisy synthetic data (blue), data from the initial model (red), and predicted data from the inversion result (black). The initial model is generated using a Dix-type phase inversion for Love waves.

step is able to find improvement. The initial and final models are defined on an optimal nonuniform grid. The improved data fit can be observed in Figure 2. Notable in this plot is that the Love-wave phase velocities over a significant part of the frequency band are lower than the Rayleigh-wave phase velocities for the MODX model shown in Haney and Tsai (2017). Such a scenario of Love waves being slower than Rayleigh waves is not typically observed at the scale of crustal seismology, but it makes sense for the strongly varying MODX model given the earlier discussion of sensitivity depth for Love waves in a power-law profile being 0.25ℓ instead of 0.5ℓ as for Rayleigh waves. Finally, in Figure 3, we plot the shear-velocity sensitivity kernel for the final update, indicating some depth resolvability down to 30 m at the lower end of the frequency band. The kernel does not display the complexity seen for the Rayleigh-wave sensitivity

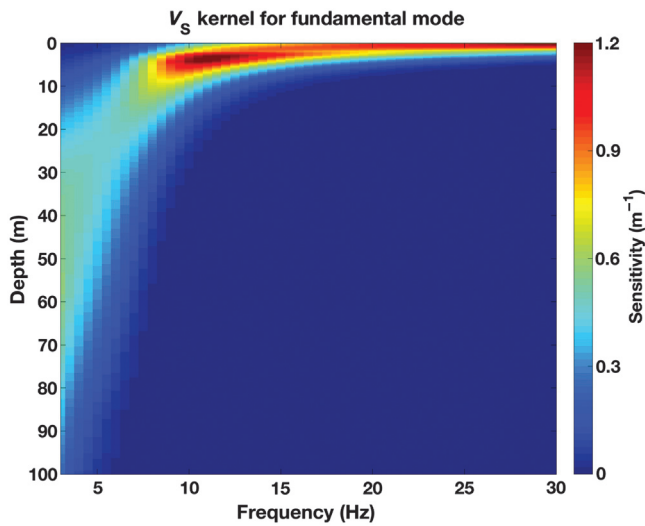


Figure 3. Fundamental-mode phase sensitivity kernel of the final inversion update for the MODX example.

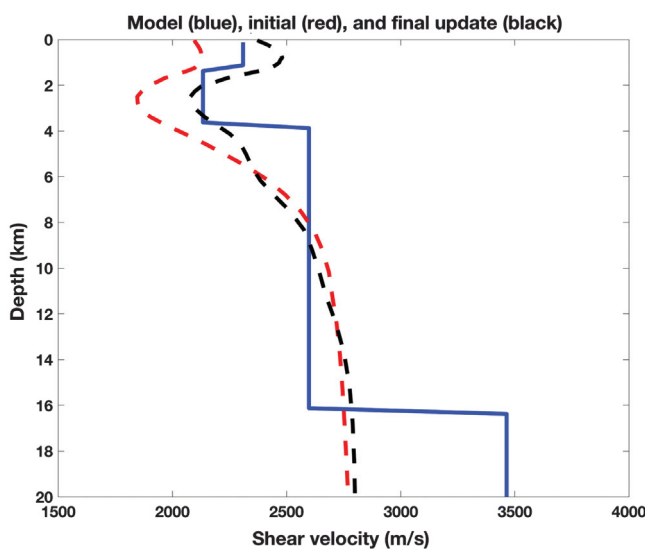


Figure 4. Shear velocity depth models for the crustal example: true model (solid blue), initial model (dashed red), and inverted model (dashed black).

kernel shown in Haney and Tsai (2017), which was due in part to a prograde-retrograde reversal for the MODX model.

The second example uses the crustal-scale model shown in Figure 4. The degree of vertical heterogeneity in the model is significantly less than the MODX model, and the main feature of interest is the subtle low-velocity zone in the second layer below the free surface. The SH-velocity model is plotted in Figure 4; for the SV model, the velocity of the second layer has been reduced by 18% to test how well the radial anisotropy can be recovered. This type of radial anisotropy has typically been detected using the discrepancy between S-wave velocity models found either using Rayleigh or Love waves (Jaxybulatov et al., 2014). To run the example, we execute the following five MATLAB scripts:

```

>> make_synthetic_ex2_rayleigh
>> make_initial_model_dix_ex2
>> make_synthetic_ex2_love
>> lovee_invert
>> plot_results_ex2

```

The first two scripts generate synthetic Rayleigh-wave phase velocities over the band from 0.1 to 0.9 Hz from the SV-velocity model and then perform Dix inversion using the homogeneous formulation for Rayleigh waves. The fundamental and first-higher modes are modeled, but only the fundamental mode is used for construction of the initial model using the Dix method. The next two scripts generate synthetic Love-wave phase velocities for the fundamental and first-higher mode from the SH-velocity model and then apply perturbational inversion to the Love-wave velocities using the initial model defined from the Rayleigh waves. The perturbational inversion is able to find an acceptable model after two iterations. Only 148 of the 159 phase velocity measurements are used for the final

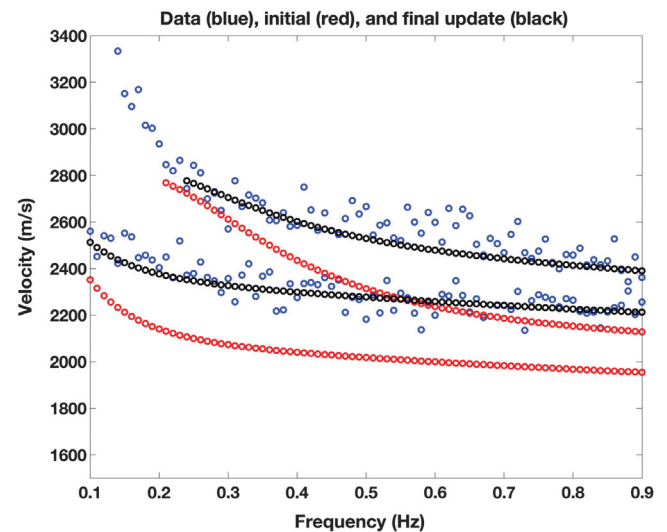


Figure 5. Phase velocity dispersion curves for the crustal example: noisy synthetic fundamental-mode and first overtone data (blue), fundamental-mode data from the initial model (red), and predicted fundamental-mode and first overtone data from the inversion result (black). In each case, the fundamental mode is always of lower velocity than the first overtone.

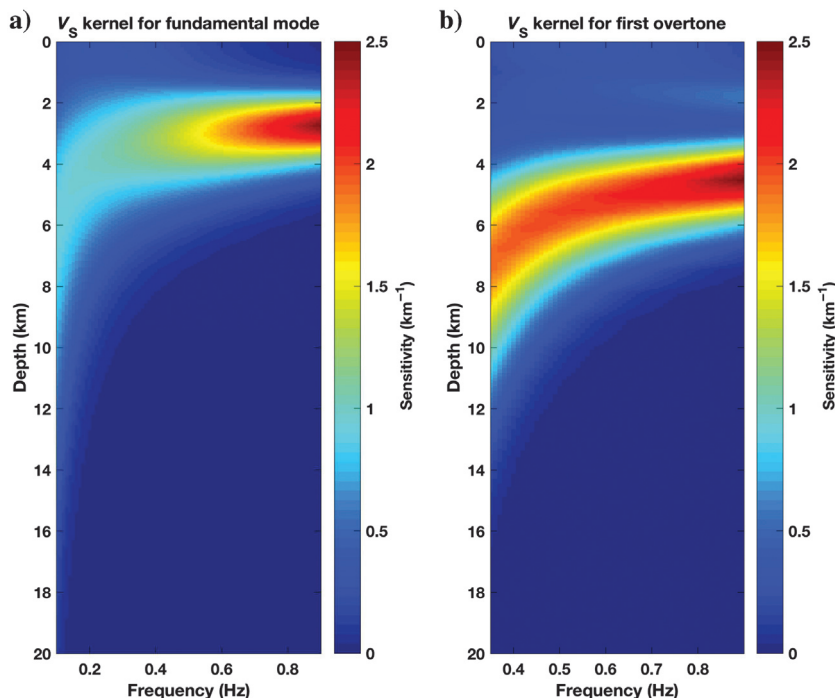


Figure 6. (a) Fundamental-mode and (b) first overtone sensitivity kernels of the final inversion update for the crustal example.

iteration because several of the higher mode measurements exist below the lower cutoff frequency of the initial model. The codes are able to automatically detect these incompatible measurements and not use them in the inversion.

The final script produces Figures 4–6 showing the relevant models, data fit, and sensitivity kernels. The Love waves improve the initial model generated from the Rayleigh waves in Figure 4 primarily by increasing the shallow S-wave velocity. The increase is consistent with the 18% reduction in the SV-velocity relative to the SH-velocity as discussed above. Note that the S-wave velocity is increased over the depth range of the first and second layers in the true model, even though the SV-velocity was actually only reduced in the second layer. The modification to the initial model by the Love waves leads to an improved fit of the fundamental and first-higher-mode data shown in Figure 5. Sensitivity kernels of the two modes for the final update are given in Figure 6 and show the complexity of Love waves in the presence of a low-velocity zone. The complexity is evident because, in contrast to the case of fundamental-mode Rayleigh waves in Haney and Tsai (2017), Love waves are more strongly channelized in the low-velocity zone. This can be seen in Figure 6 by the lack of sensitivity at the free surface for these two lowermost modes. The sensitivity kernels show why the final shear-velocity model plotted in Figure 4 is higher at shallow depths (<1 km) relative to the initial model, even though the SV-velocity is the same as the SH-velocity at those depths. It is due to a lack of sensitivity at the shallow depths and the desire for smoothness relative to the a priori model correlation length D , which has been set at 1 km for this example. In this regard, note that the first overtone has only a weak first lobe, which is barely visible, in its sensitivity kernel at a depth of approximately 2 km in Figure 6.

CONCLUSIONS

We have presented codes for the inversion of Love-wave velocities and discussed particular issues that arise for Love waves compared to Rayleigh waves. The codes can invert for any collection of phase/group velocity measurements of any Love-wave mode. An additional feature of the codes is the ability to define depth models with nonuniform layering. Two examples of inversions have been provided with the codes. The first is at the near-surface scale, for which the Love waves themselves define the initial model. The other example, at the crustal scale, refines an initial model determined from Rayleigh waves with Love-wave dispersion in the presence of radial anisotropy. Compared to Rayleigh waves, the ability to model and invert Love waves offers the advantages of not being sensitive to unknown variations in Poisson's ratio and/or the presence of a water layer above the solid portion of the model. A disadvantage of Love waves is that they do not exist for a homogeneous half-space and so their utility for defining an initial model in the presence of weak heterogeneity is limited.

ACKNOWLEDGMENTS

The comments by S. de Ridder, P. Dawson, S. Popik, and an anonymous reviewer have helped improve this manuscript and code. Any use of trade, firm, or product names is for descriptive purposes only and does not imply endorsement by the U.S. government.

DATA AND MATERIALS AVAILABILITY

No data were used in this paper.

REFERENCES

- Aki, K., and P. G. Richards, 1980, Quantitative seismology: W. H. Freeman and Company.
- Aster, R., B. Borchers, and C. Thurber, 2004, Parameter estimation and inverse problems: Elsevier Academic Press.
- Behm, M., G. M. Leahy, and R. Snieder, 2014, Retrieval of local surface wave velocities from traffic noise — An example from the La Barge basin (Wyoming): *Geophysical Prospecting*, **62**, 223–243, doi: [10.1111/1365-2478.12080](https://doi.org/10.1111/1365-2478.12080).
- Chouet, B., G. De Luca, G. Milana, P. Dawson, M. Martini, and R. Scarpa, 1998, Shallow velocity structure of Stromboli Volcano, Italy, derived from small-aperture array measurements of Strombolian Tremor: *Bulletin of the Seismological Society of America*, **88**, 653–666.
- Denolle, M. A., E. M. Dunham, and G. C. Beroza, 2012, Solving the surface-wave eigenproblem with Chebyshev spectral collocation: *Bulletin of the Seismological Society of America*, **102**, 1214–1223, doi: [10.1785/0120110183](https://doi.org/10.1785/0120110183).
- Dix, C. H., 1955, Seismic velocities from surface measurements: *Geophysics*, **20**, 68–86, doi: [10.1190/1.1438126](https://doi.org/10.1190/1.1438126).
- Gerstoft, P., K. G. Sabra, P. Roux, W. A. Kuperman, and M. C. Fehler, 2006, Green's functions extraction and surface-wave tomography from microseisms in southern California: *Geophysics*, **71**, no. 4, SI23–SI31, doi: [10.1190/1.2210607](https://doi.org/10.1190/1.2210607).
- Gouveia, W. P., and J. A. Scales, 1998, Bayesian seismic waveform inversion: Parameter estimation and uncertainty analysis: *Journal of Geophysical Research*, **103**, 2759–2779, doi: [10.1029/97JB02933](https://doi.org/10.1029/97JB02933).
- Haltiner, G. J., and R. T. Williams, 1980, Numerical prediction and dynamic meteorology: John Wiley & Sons Inc.
- Haney, M., and H. Douma, 2011, Inversion of Love wave phase velocity, group velocity and shear stress ratio using finite elements: 81st Annual

- International Meeting, SEG, Expanded Abstracts, 2512–2516, doi: [10.1190/1.3627714](https://doi.org/10.1190/1.3627714).
- Haney, M. M., 2007, Generalization of von Neumann analysis for a model of two discrete halfspaces: The acoustic case: *Geophysics*, **72**, no. 5, SM35–SM46, doi: [10.1190/1.2750639](https://doi.org/10.1190/1.2750639).
- Haney, M. M., and V. C. Tsai, 2015, Nonperturbational surface-wave inversion: A Dix-type relation for surface waves: *Geophysics*, **80**, no. 6, EN167–EN177, doi: [10.1190/geo2014-0612.1](https://doi.org/10.1190/geo2014-0612.1).
- Haney, M. M., and V. C. Tsai, 2017, Perturbational and nonperturbational inversion of Rayleigh-wave velocities: *Geophysics*, **82**, no. 3, F15–F28, doi: [10.1190/geo2016-0397.1](https://doi.org/10.1190/geo2016-0397.1).
- Hawkins, R., 2018, A spectral element method for surface wave dispersion and adjoints: *Geophysical Journal International*, **215**, 267–302, doi: [10.1093/gji/ggy277](https://doi.org/10.1093/gji/ggy277).
- Herrmann, R. B., 2013, Computer programs in seismology: An evolving tool for instruction and research: *Seismological Research Letters*, **84**, 1081–1088, doi: [10.1785/0220110096](https://doi.org/10.1785/0220110096).
- Herrmann, R. B., and C. J. Ammon, 2004, Surface waves, receiver functions and crustal structure, Computer programs in seismology, version 3.30: Saint Louis University, <http://www.eas.slu.edu/People/RBHerrmann/CPS330.html>.
- Jaxybulatov, K., N. M. Shapiro, I. Koulakov, A. Mordret, M. Landés, and C. Sens-Schönfelder, 2014, A large magmatic sill complex beneath the Toba caldera: *Science*, **346**, 617–619, doi: [10.1126/science.1258582](https://doi.org/10.1126/science.1258582).
- Jay, J. A., M. E. Pritchard, M. E. West, D. Christensen, M. Haney, E. Minaya, M. Sunagua, S. R. McNutt, and M. Zabala, 2012, Shallow seismicity, triggered seismicity, and ambient noise tomography at the long-dormant Uturuncu volcano, Bolivia: *Bulletin of Volcanology*, **74**, 817–837, doi: [10.1007/s00445-011-0568-7](https://doi.org/10.1007/s00445-011-0568-7).
- Kausel, E., 2005, Wave propagation modes: From simple systems to layered soils, in C. G. Lai and K. Wilmanski, eds., *Surface waves in geomechanics: Direct and inverse modelling for soil and rocks*: Springer-Verlag, 165–202.
- Lanza, F., L. M. Kenyon, and G. P. Waite, 2016, Near-surface velocity structure of Pacaya Volcano, Guatemala, derived from small-aperture array analysis of seismic tremor: *Bulletin of the Seismological Society of America*, **106**, 1438–1445, doi: [10.1785/0120150275](https://doi.org/10.1785/0120150275).
- Lehoucq, R. B., D. C. Sorensen, and C. Yang, 1998, ARPACK users' guide: Solution of large scale eigenvalue problems with implicitly restarted Arnoldi methods: SIAM.
- Ma, Y., and R. Clayton, 2016, Structure of the Los Angeles Basin from ambient noise and receiver functions: *Geophysical Journal International*, **206**, 1645–1651, doi: [10.1093/gji/ggw236](https://doi.org/10.1093/gji/ggw236).
- Marfurt, K. J., 1984, Accuracy of finite-difference and finite-element modeling of the scalar and elastic wave equations: *Geophysics*, **49**, 533–549, doi: [10.1190/1.1441689](https://doi.org/10.1190/1.1441689).
- Muzyert, E., 2007, Seabed property estimation from ambient-noise recordings — Part 1: Compliance and Scholte wave phase-velocity measurements: *Geophysics*, **72**, no. 2, U21–U26, doi: [10.1190/1.2435587](https://doi.org/10.1190/1.2435587).
- Nakata, N., 2016, Near-surface S-wave velocities estimated from traffic-induced Love waves using seismic interferometry with double beamforming: *Interpretation*, **4**, no. 4, SQ23–SQ31, doi: [10.1190/INT-2016-0013.1](https://doi.org/10.1190/INT-2016-0013.1).
- Paige, C. C., and M. A. Saunders, 1982, LSQR: An algorithm for sparse linear equations and sparse least squares: *Association for Computing Machinery Transactions on Mathematical Software*, **8**, 43–71, doi: [10.1145/355984.355989](https://doi.org/10.1145/355984.355989).
- Rodi, W. L., P. Glover, T. M. C. Li, and S. S. Alexander, 1975, A fast, accurate method for computing group-velocity partial derivatives for Rayleigh and Love modes: *Bulletin of the Seismological Society of America*, **65**, 1105–1114.
- Saito, M., 1988, Disper80, in D. J. Doornbos, ed., *Seismological algorithms: Computational methods and computer programs*: Academic Press, 293–319.
- Sniieder, R., and J. Trampert, 1999, Inverse problems in geophysics, in A. Wirgin, ed., *Wavefield inversion*: Springer Verlag, 119–190.
- Takeuchi, H. M., and M. Saito, 1972, Seismic surface waves, in B. A. Bolt, ed., *Methods in computational physics*: Academic Press, 217–295.
- Tarantola, A., and B. Valette, 1982, Generalized nonlinear inverse problems solved using the least squares criterion: *Reviews of Geophysics and Space Physics*, **20**, 219–232, doi: [10.1029/RG020i002p00219](https://doi.org/10.1029/RG020i002p00219).
- Tsai, V. C., and S. Atiganyanun, 2014, Green's functions for surface waves in a generic velocity structure: *Bulletin of the Seismological Society of America*, **104**, 2573–2578, doi: [10.1785/0120140121](https://doi.org/10.1785/0120140121).
- Xia, J., R. D. Miller, and C. B. Park, 1999, Estimation of near-surface shear-wave velocity by inversion of Rayleigh waves: *Geophysics*, **64**, 691–700, doi: [10.1190/1.1444578](https://doi.org/10.1190/1.1444578).
- Xia, J., Y. Xu, Y. Luo, R. D. Miller, R. Cakir, and C. Zeng, 2012, Advantages of using multichannel analysis of love waves (MALW) to estimate near-surface shear-wave velocity: *Surveys in Geophysics*, **33**, 841–860, doi: [10.1007/s10712-012-9174-2](https://doi.org/10.1007/s10712-012-9174-2).